Chinese Chemical Letters 34 (2023) 107650

Contents lists available at ScienceDirect

Chinese Chemical Letters

journal homepage: www.elsevier.com/locate/cclet

An ultra-highly active nanozyme of Fe,N co-doped ultrathin hollow carbon framework for antibacterial application

Jinyu Hao[a], Cui Zhang[c], Chenxi Feng[a], Qian Wang[a], Zhong-Yi Liu[a], Yan Li[a], Jianshuai Mu[a,*], En-Cui Yang[a,*], Yan Wang[b,*]

[a] College of Chemistry, Tianjin Key Laboratory of Structure and Performance for Functional Molecules, Tianjin Normal University, Tianjin 300387, China
[b] School of Chemistry and Chemical Engineering, Harbin Institute of Technology, Harbin 150001, China
[c] School of food and Bioengineering, Xuzhou University of Technology, Xuzhou 221018, China

ARTICLE INFO

Article history:
Received 8 March 2022
Revised 23 June 2022
Accepted 27 June 2022
Available online 30 June 2022

Keywords:
Peroxidase-like
Nanozyme
Ultra-highly active
Specific activity
Antibacterial

ABSTRACT

In recent years, nanozymes have received more and more attention, but the low activity limits the development of nanozymes. Therefore, the design and development of efficient nanozymes is still a major challenge for researchers. Herein, the Fe,N co-doped ultrathin hollow carbon framework (Fe,N-UHCF) exhibit ultra-high peroxidase-like activity. The specific activity of Fe,N-UHCF nanozyme is as high as 36.6 U/mg, which is much higher than almost all of other reported nanozymes. In practical applications, the Fe,N-UHCF show good antibacterial effects.

Natural enzymes are a class of biomolecules, which can effectively catalyze various specific biochemical reactions, control the metabolism, nutrition and energy conversion process of the body [1–3]. Therefore, they play an important role in organisms, and have a wide range of applications in the field of biomedical [4–6]. However, the high cost, difficult preparation, instability and other problems of natural enzymes seriously restrict their practical application. Therefore, artificial mimetic enzymes are one of the important topics in recent decades [7–10].

Nanozymes as nanomaterials endowing with enzyme-like activity are a new type of artificial enzymes. The potential alternatives of nanozymes as natural enzymes have caused extensive attention in catalytic fields [11–14]. Compared with natural enzymes, nanozymes have the advantages of good stability, low cost, and easy-scale production. Therefore, they are ideal substitutes for natural enzymes and are suitable for various applications [15,16]. Since the pioneering work reported by Yan's group [17], many nanozymes have been developed for various applications, ranging from analytical detection, environmental remediation to therapeutic applications [18,19]. A series of nanozymes including peroxidase, oxidase, superoxide dismutase, catalase and so on have been explored up to now [20,21]. Although nanozymes have made significant progress, their development is hindered by problems such as relatively low activity, poor specificity, and uncertain catalytic mechanism [22–25]. Therefore, the design and development of efficient nanozymes is still a major challenge.

Bacterial infectious diseases is one of the biggest health problems worldwide, afflicting millions of people every year [26]. At present, treatment is heavily dependent on antibiotics. Due to the dependence on antibiotics, many kinds of drug-resistant 'superbacteria' continue to appear, and the treatment effect has dropped sharply [27,28]. Huge efforts have been made to develop alternative antibacterial materials. In recent years, nanozyme-based antibacterial therapy has become a new generation of antibiotics due to its extensive antibacterial activity, negligible toxicity and lack of resistance to nanozymes [29]. Inspired by natural enzymes that destroy bacteria by catalyzing the production of harmful reactive oxygen species (ROS), nanozymes can convert H_2O_2 or O_2 into highly toxic hydroxyl radicals (•OH) for the treatment of bacterial infections [30,31].

Herein, in order to obtain high activity of nanozyme, the Fe,N co-doped ultrathin hollow carbon framework (Fe,N-UHCF) with high content of Fe-N_x bonding and unique morphology were synthesized. The Fe,N-UHCF exhibit ultra-high peroxidase-like activity, which is much higher than almost all of other reported nanozymes. And its antibacterial effects were also investigated.

Using silicon spheres as a template, the Fe,N-UHCF was synthesized by a one-pot high-temperature calcination method using

* Corresponding authors.
E-mail addresses: hxxymujianshuai@tjnu.edu.cn (J. Mu), encui_yang@163.com (E.-C. Yang), wangy_msn@hit.edu.cn (Y. Wang).

https://doi.org/10.1016/j.cclet.2022.06.073
1001-8417/

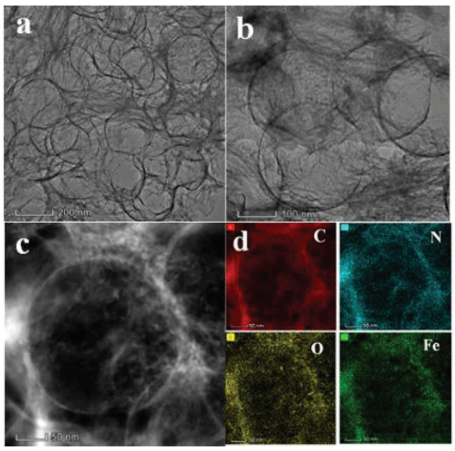

Fig. 1. (a, b) TEM images of Fe,N-UHCF and (c) the corresponding low-magnification HAADF-STEM image, (d) EDS mapping images of C, N, O and Fe.

porous carbon (PC), iron nitrate, glucose and dicyandiamide as carbon substrate, Fe source, chelating agent and nitrogen source. The crystal structure of Fe,N-UHCF and N doped carbon (N–C) was characterized by XRD. Similar to N–C, the XRD pattern of Fe,N-UHCF shows a broad diffraction peak and no other peaks (Fig. S1 in Supporting information). This implies no formation of crystallized Fe species except for amorphous carbon. The morphology of Fe,N co-doped carbon (Fe,N–C), N-doped ultrathin hollow carbon framework (N-UHCF) and Fe,N-UHCF was characterized by transmission electron microscope (TEM). It shows that the morphology of Fe,N–C and N-UHCF is nanosheet and hollow spherical framework, respectively (Figs. S2a and b in Supporting information). The electron dispersive spectra (EDS) mapping images indicate the uniform distributions of C, N, and O in the whole architecture of N-UHCF (Fig. S2c in Supporting information). The morphology of Fe,N-UHCF exhibits amounts of hollow spherical framework after removal of silica spheres templates, with an ultrathin shell thickness of ~4 nm (Figs. 1a and b). And the surface of hollow spheres is covered with a layer of lamellar and flocculent structure, which may be composed of PC substrate and glucose pyrolysis. The big Fe-based particles are not observed during the TEM images. The electron dispersive spectra (EDS) mapping images indicate the uniform distributions of C, N, O, and Fe in the whole architecture of Fe,N-UHCF (Figs. 1c and d). The above results verify that Fe is successfully doped into the hollow carbon spheres. Measured by inductively coupled plasma atomic emission spectrometry (ICP-AES), the actual Fe loading is 5.85 wt%. The chemical enviroments of Fe,N-UHCF and Fe,N co-doped carbon (Fe,N–C) were investigated by X-ray photoelectron spectroscopy (XPS) (Fig. S3 in Supporting information). The C 1s spectra show the existence of C–C, C=C, C–N and C=O [32]. The N 1s signals indicate the presence of pyridinic N, Fe-N_x species, pyrrolic N, graphitic N and oxidized N, in which the peak at 399.5 eV is assigned to Fe-N_x species [25]. The Fe 2p spectra of Fe,N-UHCF and Fe,N–C have two peaks at 711.1 and 724.7 eV, indicating the presence of oxidized Fe [24]. The O 1s spectra consist of two peaks labelled as O1 and O2, corresponding to the oxygen defects and chemisorbed species (such as H_2O or O_2), respectively [33]. Moreover, in the O 1s spectra there is no distinct features of Fe-O bonding, which should appear around 530 eV [25]. The above XPS analysis show that Fe-N_x bonding is the dominant Fe species in Fe,N-UHCF and Fe,N–C. Compared with Fe,N–C, the Fe,N-UHCF have larger amount of Fe-N_x bonding, which may provide more active sites and contribute to the improvement of catalytic performance. The BET specific surface areas of Fe,N-UHCF and Fe,N–C were measured to be 502.1 m^2/g and 180.6 m^2/g, respectively (Fig. S4 in Supporting information). The unique hollow structure enables Fe,N-UHCF to have a larger specific surface area, which can expose more active sites, and be conducive to efficient mass transfer.

The typically chromogenic reaction of 3,3′,5,5′-tetramethylbenzidine (TMB) oxidized by H_2O_2 can be used to verify the peroxidase activity of catalysts. In absence of catalyst, H_2O_2 cannot oxidize TMB (Fig. 2a). After adding the N–C catalyst, TMB is oxidized, and the solution is slightly blue, which corresponds to the absorption peak at 652 nm measured by the UV–vis spectrophotometer. While in presence of N-UHCF, the blue of the solution deepened. The result shows that the morphology of hollow spherical framework greatly increases the peroxidase-like activity of the catalysts. While in presence of Fe,N–C, the solution turns blue obviously, and the absorption peak is much larger than that of N–C as the catalyst. It shows that the Fe doping greatly enhances the peroxidase-like activity of the catalysts. Most importantly, the Fe,N-UHCF exhibits highest peroxidase-like activity, indicating that the synergistic effect of Fe doping and unique ultrathin hollow framework greatly enhances the catalytic performance of the catalyst. The above results indicate that specific ultrathin hollow framework can expose more Fe-N_x catalytic sites, thus greatly improve its catalytic activity. The effect of Fe-doped content on their activity was investigated (Fig. S5a in Supporting information). The results show that the activity first increases and then decreases with the increase of Fe-doped content. The decrease of activity may be attributed to Fe aggregation at a higher doping. And the optimum Fe content was 5.85%. Therefore, we chose Fe,N-UHCF with Fe content of 5.85% for the following research. With the increase of Fe,N-UHCF concentration, the peroxidase-like activity of catalytic system increases gradually, showing a good linear relationship (Fig. S5b in Supporting information).

In order to study the effect of pH on the peroxidase-like activity of Fe,N-UHCF, the reaction at different pH from 3 to 8 was measured. As shown in Fig. S6a (Supporting information), the catalytic activity of Fe,N-UHCF is dependent on pH. The Fe,N-UHCF exhibits the highest catalytic activity at pH 5. More importantly, the catalytic activity only decreases a little below pH 5. Even under neutral conditions, the Fe,N-UHCF still retains the catalytic activity. The above results indicate that Fe,N-UHCF exhibits good performance at a wide pH range, which is rarely reported in the literatures. The effect of temperature on the mimetic peroxidase activity of Fe,N-UHCF was investigated at temperature from 20 °C to 60 °C. The catalytic activity of Fe,N-UHCF is closely related to temperature, and the optimum temperature is 40 °C (Fig. S6b in Supporting information). Notably, the Fe,N-UHCF still maintains efficient catalytic activity even at a high temperature of 60 °C, indicating that the Fe,N-UHCF nanozyme has a wide range of temperature adaptation.

The specific activity of Fe,N-UHCF was evaluated according to the standardized protocol [34]. By choosing 60 s as the initial rate period, the catalytic activity of Fe,N-UHCF expressed in units (U) was then calculated (Fig. S7 in Supporting information). After adding the nanozymes, the catalytic activity increases linearly with the added amount of nanozymes (Fig. 2b). The specific activity of Fe,N-UHCF as peroxidase nanozyme is calculated to be 36.6 U/mg, which is nearly 6 times higher than that of N-C (6.3 U/mg), and nearly 2.5 times higher than that of Fe,N-C (15.2 U/mg). The specific activity of this Fe,N-UHCF nanozyme is much higher than most of reported nanozymes (Table S1 in Supporting information). The high specific activity of Fe,N-UHCF may be originated from the following factors: On the one hand, the unique ultrathin hollow framework of Fe,N-UHCF exhibits much larger BET specific surface area (502.1 m^2/g) than that of Fe,N-C (180.6 m^2/g), and the large specific surface area can help fast mass transfer. On the other hand, the Fe,N-UHCF exposes more Fe-N_x active sites, which greatly enhance its catalytic performance. All in all, the unique morphology

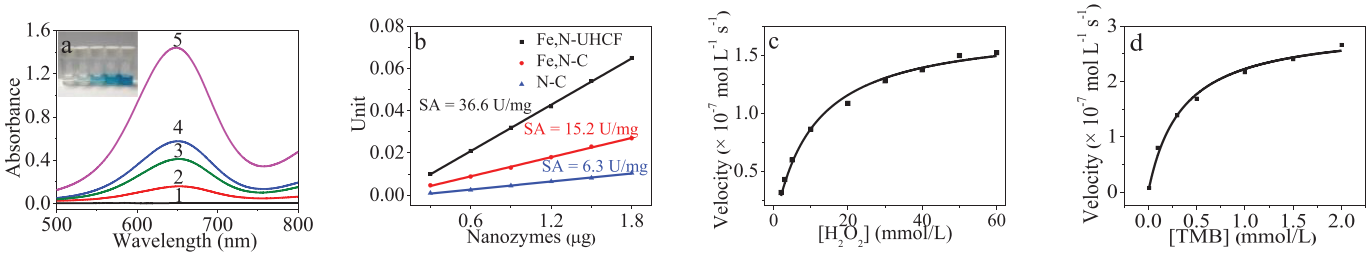

Fig. 2. (a) UV–vis absorption spectra of (1) H_2O_2 + TMB, (2) NC + H_2O_2 + TMB, (3) N-UHCF + H_2O_2 + TMB, (4) Fe,N–C + H_2O_2 + TMB, (5) Fe,N-UHCF + H_2O_2 + TMB, insert shows the color change of these systems, reaction for 5 min. (b) The specific activities (U/mg) of Fe,N-UHCF, Fe,N-C and N-C. (c, d) The steady-state kinetics curves of Fe,N-UHCF toward H_2O_2 and TMB, respectively.

and high content of Fe-N_x active sites (Fe doping) endow the Fe,N-UHCF nanozyme with ultra-high specific activity.

The catalytic performance of Fe,N-UHCF was further studied by steady-state kinetic. Firstly, at a fixed concentration of TMB, the catalytic kinetics curves under different H_2O_2 concentrations were measured (Fig. S8a in Supporting information). With the increase of H_2O_2 concentration, the initial reaction rate gradually increases. And the growth rate flattens out at a high concentration of H_2O_2 (Fig. 2c). Then, the catalytic kinetic curves at different TMB concentrations with a fixed concentration of H_2O_2 were measured (Fig. S8b in Supporting information). The initial reaction rate increases with the increase of TMB concentration, and tends to the highest value at a high TMB concentration (Fig. 2d). The kinetic curves of the Fe,N-UHCF under the substrates TMB and H_2O_2 indicate that the catalytic reaction follows the typical Michaelis-Menten kinetics. Using the Lineweaver-Burk equation to fit the data of the Michaelis-Menten curves, the Lineweaver-Burk plots were obtained (Figs. S8c and d in Supporting information). According to the slopes and intercepts, the kinetic parameters including K_m and V_{max} were calculated (Table S2 in Supporting information). K_m represents the affinity of the enzyme toward the substrate. The smaller the K_m value, the higher the enzyme's affinity toward the substrate. The K_m value of the Fe,N-UHCF toward TMB is smaller than the other reported nanozymes, indicating that the Fe,N-UHCF have a much higher binding ability toward TMB. While the K_m value of the Fe,N-UHCF toward H_2O_2 is the same order of magnitude as that of HRP. The kinetic results show that the Fe,N-UHCF exhibits good affinity for the substrates.

In order to further explore the high peroxidase activity of Fe,N-UHCF, the catalytic mechanism was investigated. The production of hydroxyl radicals (•OH) was monitored by the luminescence experiment with terephthalic acid (TA). As a typical fluorescent probe, TA can capture •OH, resulting in strong fluorescence. As shown in Fig. 3a, there is a significant fluorescence signal in presence of both Fe,N-UHCF and H_2O_2. As the concentration of the nanozyme increased, the stronger fluorescence signals indicate the production of more •OH (Fig. 3a). Therefore, the Fe,N-UHCF can catalyze H_2O_2 to produce •OH, which oxidizes the organic substrate TMB to produce color changes, resulting in its peroxidase-like activity.

P. aeruginosa, widely distributed in humid environments, is one of the main pathogens of hospital infections. It can spread diseases and pose a huge threat to human health. According to reports, highly toxic reactive oxygen species (ROS) including •OH can effectively kill bacteria [21]. The above results show that Fe,N-UHCF nanozyme can catalyze the generation of •OH from H_2O_2. Encouraged by the excellent performance of Fe,N-UHCF nanozyme, its antibacterial application against *P. aeruginosa in vitro* was studied. For *in vitro* antibacterial experiments, the plate count method was used to determine the antibacterial activity of Fe,N-UHCF against *P. aeruginosa* (Fig. 3b and Figs. 4a-d). The growth inhibition rate of H_2O_2 alone against *P. aeruginosa* is only 24.9%, while the growth inhibition rate of Fe,N-UHCF in absence of H_2O_2 increases to 66.3%. In the presence of H_2O_2, the Fe,N-UHCF shows a high antibacterial effect against *P. aeruginosa*, with inhibiting growth by up to 91.5%. The high antibacterial activity of Fe,N-UHCF is due to its efficient nanozyme activity to generate •OH. To further decipher the antibacterial behavior, TEM images were used to study the morphological changes of *P. aeruginosa* (Figs. 4e-h). *P. aeruginosa* is rod-shaped with smooth surface, and its length of about 1 μm (Fig. 4e). In presence of H_2O_2 alone, there is no obvious change, indicating the negligible damage to the bacteria (Fig. 4f). After treatment with Fe,N-UHCF, a few disruptions can be observed on the bacterial cell walls (Fig. 4g). However, after exposed to Fe,N-UHCF + H_2O_2, the bacterial cell wall becomes wrinkled and incomplete, and the length of the bacteria is reduced to about 700~800 nm, indicating a stronger antibacterial ability of the synergistic system (Fig. 4h). The above results demonstrate that the Fe,N-UHCF is a superior nanozyme for effective antibacterial application.

In summary, a highly active Fe,N-UHCF nanozyme was successfully constructed using a one-pot high-temperature calcination method, which overcomes the challenges faced by nanozymes with low activity in the past. The specific activity of Fe,N-UHCF is much

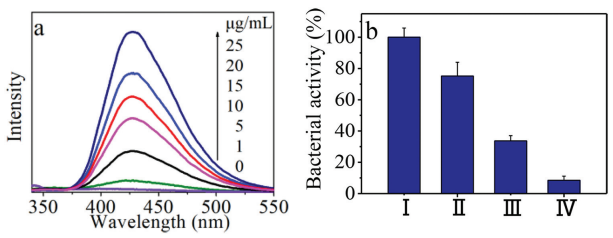

Fig. 3. (a) The effect of the amount of Fe,N-UHCF on the generation of the hydroxyl radical by H_2O_2 with terephthalic acid (TA) as a fluorescent probe, (b) Bacterial activity of *P. aeruginosa* bacteria after treatments of (I) control; (II) H_2O_2 (100 μmol/L); (III) Fe,N-UHCF (200 μg/mL); (IV) Fe,N-UHCF (200 μg/mL) + H_2O_2 (100 μmol/L) at pH 4.5. The data were based on three parallel experiments (Mean ± SD, $n = 3$, * $P < 0.05$, ** $P < 0.01$, *** $P < 0.001$ compared to control group).

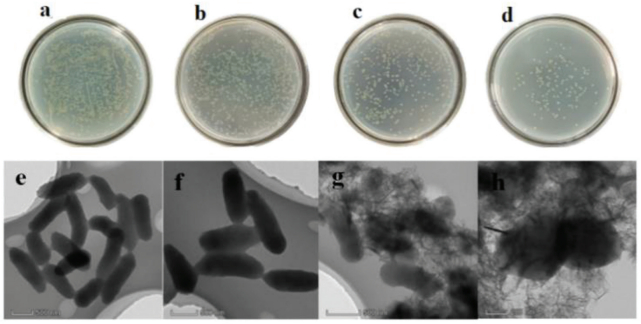

Fig. 4. (a-d) Photographs of the remaining *P. aeruginosa* bacteria in agar plates (a. control; b. H_2O_2; c. Fe,N-UHCF; d. Fe,N-UHCF + H_2O_2). TEM images of *P. aeruginosa* bacterial colonies treated with (e) control, (f) H_2O_2, (g) Fe,N-UHCF, (h) Fe,N-UHCF + H_2O_2.

higher than most of other reported nanozymes. The untra-high activity is from the unique ultrathin hollow framework and high loading of Fe-N_x bonding. Based on the excellent nanozyme activity, the Fe,N-UHCF was applied to *in vitro* antibacterial applications, showing good antibacterial effects. This provides a new way for the rational design of efficient nanozymes.

Declaration of competing interest

There are no conflicts to declare.

Acknowledgments

This work was supported by the National Natural Science Foundation of China (NSFC, Nos. 21671149, 21571140, 21531005 and 21703156), the 973 Program (No. 2014CB845601), the Program for Innovative Research Team in University of Tianjin (No. TD13–5074), the Natural Science Foundation of Tianjin (No. 18JCQNJC76000), the Science & Technology Development Fund of Tianjin Education Commission for Higher Education (No. 2021KJ190), the Jiangsu Provincial Double-Innovation Doctor Program (No. 02300053).

Supplementary materials

Supplementary material associated with this article can be found, in the online version, at doi:10.1016/j.cclet.2022.06.073.

References

[1] Y.H. Hu, X.J.J. Gao, Y.Y. Zhu, et al., Chem. Mater. 30 (2018) 6431–6439.
[2] C. Zhao, C. Xiong, X.K. Liu, et al., Chem. Commun. 55 (2019) 2285–2288.
[3] Y.P. Chen, Y.L. Xianyu, M.L. Dong, et al., Anal. Chem. 90 (2018) 6906–6912.
[4] E.N. Mirts, I.D. Petrik, P. Hosseinzadeh, et al., Science 361 (2018) 1098–1101.
[5] Y.B. Zhou, B.W. Liu, R.H. Yang, et al., Bioconjugate Chem. 28 (2017) 2903–2909.
[6] F.M. Wang, Y. Zhang, Z.W. Liu, et al., Nanoscale 12 (2020) 14465–14471.
[7] Y.H. Lin, J.S. Ren, X.G. Qu, Acc. Chem. Res. 47 (2014) 1097–1105.
[8] X.L. Zhang, G.L. Li, D. Wu, et al., Biosens. Bioelectron. 137 (2019) 178–198.
[9] J.J.X. Wu, X.Y. Wang, Q. Wang, et al., Chem. Soc. Rev. 48 (2019) 1004–1076.
[10] M.M. Liang, X.Y. Yan, Acc. Chem. Res. 52 (2019) 2190–2200.
[11] L.L. Zeng, Y.X. Han, Z.W. Chen, et al., Adv. Sci. 8 (2021) 2101184.
[12] W.J. Ma, Y.F. Xue, S.Y. Guo, et al., Chem. Commun. 56 (2020) 5115–5118.
[13] D.M. He, M.M. Yan, P.J. Sun, et al., Chin. Chem. Lett. 32 (2021) 2994–3006.
[14] Z.J. Zhang, L.M. Bragg, M.R. Servos, et al., Chin. Chem. Lett. 30 (2019) 1655–1658.
[15] W.H. Chen, M. Vazquez-Gonzalez, A. Kozell, et al., Small 14 (2018) 1703149.
[16] M.J. Lu, C. Wang, Y.Q. Ding, et al., Chem. Commun. 55 (2019) 14534–14537.
[17] L.Z. Gao, J. Zhuang, L. Nie, et al., Nat. Nanotechnol. 2 (2007) 577–583.
[18] L. Han, H.J. Zhang, D.Y. Chen, et al., Adv. Funct. Mater. 28 (2018) 1800018.
[19] S.Q. Li, Y.J. Hou, Q.M. Chen, et al., ACS Appl. Mater. Interfaces 12 (2020) 2581–2590.
[20] X.H. Niu, Q.R. Shi, W.L. Zhu, et al., Biosens. Bioelectron. 142 (2019) 111495.
[21] Y.Y. Zhong, T.T. Wang, Z.T. Lao, et al., ACS Appl. Mater. Interfaces 13 (2021) 21680–21692.
[22] L. Jiao, W.Q. Xu, Y. Zhang, et al., Nano Today 35 (2020) 100971.
[23] J.Q. Zhang, Y.F. Zhao, C. Chen, et al., J. Am. Chem. Soc. 141 (2019) 20118–20126.
[24] L. Jiao, W.Q. Xu, H.Y. Yan, et al., Anal. Chem. 91 (2019) 11994–11999.
[25] L. Zhao, Y. Zhang, L.B. Huang, et al., Nat. Commun. 10 (2019) 1278.
[26] Y.J. Sang, W. Li, H. Liu, et al., Adv. Funct. Mater. 29 (2019) 1900518.
[27] M.F. Huo, L.Y. Wang, H.X. Zhang, et al., Small 15 (2019) 1901834.
[28] L.W. Wang, F.N. Gao, A.Z. Wang, et al., Adv. Mater. 32 (2020) 2005423.
[29] F.F. Cao, L. Zhang, H. Wang, et al., Angew. Chem. Int. Ed. 58 (2019) 16236–16242.
[30] H.J. Xiang, W. Feng, Y. Chen, Adv. Mater. 32 (2020) 1905994.
[31] B.L. Xu, H. Wang, W.W. Wang, et al., Angew. Chem. Int. Ed. 58 (2019) 4911–4916.
[32] W.X. Chen, J.J. Pei, C.T. He, et al., Angew. Chem. Int. Ed. 56 (2017) 16086–16090.
[33] V. Kumar, H.C. Swart, O.M. Ntwaeaborwa, et al., Mater. Lett. 101 (2013) 57–60.
[34] B. Jiang, D.M. Duan, L.Z. Gao, et al., Nat. Protoc. 13 (2018) 1506–1520.